Retrieval of Surface Di ectional Reflectance and Hemispherical Albedo Using Multi-angle Measuren ents. I. Ground Level Observations

John V. Martonchik

Mai Stop 83-301

Jet Propulsion aboratory, California Institute of Technology

4800 Oak Grove Drive

Pasadena, CA 91109, USA

Su mi ted to: *Remote Sensing of Environment*

November, 1993

ABSTRACT

Knowledge of the directional reflectance properties of natural surfaces such as soils and vegetation canopies is essential for classification studies and canopy model inversion. Atmospheric correction schemes, using various levels of approximation, are described to retrieve surface bidirectional reflectance factors (BRFs) and directional-hemispherical reflectances (albedos) from multi-angle radiance measurements taken at ground level. The retrieval schemes are tested on simulated data incorporating realistic surface BRFs and atmospheric models containing aerosols. Sensitivity of the atmospherically-corrected BRFs and associated hemispherical reflectances to various aerosol properties and the sun-view geometry is illustrated. A measurement strategy for obtaining highly accurate surface reflectance properties also is examined in the context of instrument radiometric calibration, knowledge of the atmospheric properties and sun-view angular coverage.

INTRODUCTION

It is wel known that natural surfaces do not behave as lambertian scatterers but exhibit anisotropic reflectance properties which depend on the characteristics of the surface. In general, the reflected radiance from a given target is a function of the solar zenith angle, the viewing zenith angle and the difference between the solar and viewing azimuth angles. Measurements of directional reflected radiation then can be analyzed by means of physical surface models which provide information about the physical and optica properties of the surface (e.g., Pinty and Verstraete, 1991; 1992). The initial step in the analysis includes removing all effects of he atmosphere from the measurements (termed an atmospheric correction), resul ing in surface bidirectional reflectances as produced by a beam of unattenuated direct sunlight These reflectances then can be fitted to physical surface models ypically through adjustment of a small number of parameters. Integration of these reflectances over the whole hemisphere of viewing angles defines the directional-hemispherical reflectance (albedo) of the surface. The surface albedo is an important parameter in a global sense because it is a factor in adiation balance studies, involving energy deposition, surface temperature, and evapotranspiration (Dickinson et al., 1990; Mintz, 1984; Charney et al., 1977).

Global, regional and local area determinations of surface reflectance can only be accomplished effectively through the use of remote sensing platforms, either space-based or airborne. However, supplementary ground-based reflectance measurements frequently are made at selected sites within the field of view of the remote sensing platform so that the surface products retrieved from the platform data can be validated. Therefore, it is important that the retrieval process, performed on the ground-based reflectance measurements to correct for atmospheric effects, be as accurate as possible. This correction is required because diffuse sky radiance incident upon the surface results in a different angular distribution of the reflected radiance relative to what would be observed in the presence of only direct illumination.

In this paper results of a study are presented concerned with the surface reflectance retrieval process and some of the issues which can affect its accuracy. The accuracy issues fall into three basic categories: radiometric calibration of the sensor, knowledge of the atmospheric condition, and completeness of the angular geometry of the measurements. In this study radiometric calibration of the sensor and knowledge of the atmospheric condition initially are assumed to be perfect, and the focus is centered on the degradation of retrieval accuracy due to a limited range of angular geometry associated with the measurement set. In particular, simulated surface reflectance data sets are constructed utilizing a coupled surface-atmosphere radiative transfer code and including realistic surface bidirectional reflectance distribution functions and atmospheres with multiple scattering aerosols. These data sets, computed for selected view zenith angles, solar zenith angles and relative azimuth angles, then are used in surface reflectance retrieval algorithms employing various degrees of approximation. The dependence of the retrieval accuracies of these various algorithms on atmospheric properties and sun position is investigated for a number of different trial cases. The issues of radiometric calibration and knowledge of the atmospheric properties and their effect on surface retrievals are also considered in some detail.

BACKGROUND

For a radiometrically calibrated instrument, the measured directionally reflected radiance L at ground level from a surface target can be written as

$$L(-\mu, \mu_0, \phi - \phi_0) = \pi^{-1} \int_0^1 \int_0^{2\pi} r(-\mu, \mu', \phi - \phi') L^{inc}(\mu', \mu_0, \phi' - \phi_0) \mu' \, d\mu' \, d\phi' \qquad (1)$$

where μ and μ_0 are the cosines of the view and solar zenith angles and $\phi - \phi_0$ is the view azimuthal angle with respect to the principal plane of the sun. The convention $-\mu$ and $+\mu$ is used for upwelling and downwelling radiation respectively. On the right-hand-side of (1) L^{inc} is the total (direct and downward diffuse) radiance incident on the surface and r is the bidirectional reflectance factor

(11)< 1') of the surface target. The BRF of the surface target is defined as the bidirectional reflectance distribution function (BRDF) of the target ratioed to the BRDF of an ideal lambertian scattering surface (equal to $1/\pi$) (Nicodemus et al., 1977). It is assumed in this study that there is sufficient knowledge of the state of the atmosphere such that the atmosphere-dependent function I^{inc} in (1) can be calculated to an arbitrary degree of accuracy. Then, given L at a number of different view angles, the problem is to retrieve r, the only unknown parameter, at the same view angles as L.

There are a number of instruments available which can measure directionally reflected radiation at the surface. One instrument in particular, the Portable Apparatus for Rapid Acquisition of Bidirectional observations of the Land and Atmosphere (PARABOLA), has been used in a number of field studies (Deering and Leone, 1986). It is an automated, motorized radiometer which takes data in three wavelength bands (660, 825, and 1655 nm) and systematically makes measurements over both the downward and upward hemispheres with a 15° field-of-view. The PARABOLA data are usually expressed as experimental directional reflectance factors (or more precisely, hemispherical-conical reflectance factors for non-isotropic incident radiation (Nicodemus et al., 1977)), obtained by ratioing the radiant flux with the instrument's field-of-view reflected from the surface target to a reference radiant flux measured at essentially the same time. This reference radiant flux usually is either the reflected radiant flux in the nadir direction from a calibrated near-lambertian (e.g., $BaSO_4$ or halon) reference panel or $1/\pi$ times the incident irradiance at the surface, a quantity derived from the upward-looking hemisphere measurements (downward diffuse radiance) and ancillary sun photometer data (direct solar irradiance).

Other instruments have been used in the field to measure directionally reflected radiation at the surface but the angular coverage was usually restricted in comparison to PARABOLA. For example, Starks et al. (1991) used an MMR (Modular Multiband Radiometer) in the FIFE campaign to measure reflected radiation from prairie vegetation but the view zenith angle range was limited to 50° on both sides of nadir and the azimuth angle coverage was only in the principal plane of the sun. In this study only those measurements sets which exhibit relatively complete sky coverage like PARABOLA are considered.

RETRIEVAL ALGORITHMS

The surface BRF retrieval algorithm described here makes use of an iteration approach which can accommodate the full hemispheric angular coverage of PARABOLA-like instruments. In order that multiple reflections of radiation between the surface and the atmosphere can be taken fully into account in the algorithm, it is assumed that the reflection properties of the terrain surrounding the target area are the same as the target area. Thus, reflectance measurements are assumed to be made on a fairly homogeneous surface region with sufficient horizontal extent.

Rigorous approach

In the first step of the algorithm development, the radiance incident on the surface L^{inc} is separated into its direct and diffuse components, allowing (1) to be written as

$$L(-\mu, \mu_0, \phi-\phi_0) = \pi^{-1} r(-\mu, \mu_0, \phi-\phi_0) E_{dir}(\mu_0) + L_{diff}(-\mu, \mu_0, \phi-\phi_0). \tag{2}$$

Here E_{dir} is the direct incident irradiance at the surface and L_{diff} is the upward diffuse radiance,

$$L_{diff}(-\mu, \mu_0, \phi-\phi_0) = \pi^{-1} \int_0^1 \int_0^{2\pi} r(-\mu, \mu', \phi-\phi')\ L_{diff}^{inc}(\mu', \mu_0, \phi'-\phi_0)\ \mu'\, d\mu'\, d\phi' \tag{3}$$

with L_{diff}^{inc} as the diffuse component of the downward radiance at the surface.

Using (2), the nth iteration of the retrieval algorithm for r then can be formally written as

$$r^{(n)}(-\mu, \mu_0, \phi-\phi_0) = \frac{L(-\mu, \mu_0, \phi-\phi_0) - L_{diff}^{(n-1)}(-\mu, \mu_0, \phi-\phi_0)}{\pi^{-1} E_{dir}(\mu_0)} \tag{4}$$

where $L_{diff}^{(n-1)}$ is computed using the (n-1)th iteration of r in (3). Various expressions for the initial estimate of the BRF, $r^{(0)}$, can be derived depending on the assumptions used. The simplest form assumes that the downward diffuse radiance is negligible compared to the direct downward radiance and that atmosphere-surface reflections can be ignored. Then solving for r directly,

$$r^{(0)}(-\mu, \mu_0, \phi-\phi_0) = \frac{L(-\mu, \mu_0, \phi-\phi_0)}{\pi^{-1} E_{dir}(\mu_0)} \tag{5}$$

For subsequent iterations L_{diff}^{inc} in (3) must be updated in addition to r, since the downward diffuse radiance field normally includes multiple reflections between the surface and the atmosphere. Thus, for example, $L_{diff}^{(n-1)}$ in (4) is computed from (3) where L_{diff}^{inc} uses $r^{(n-1)}$ to describe the surface BRF.

Note that r, described by (4) or (5), is evaluated only at the reflectance (view) angles and incidence (sun) angle of the particular measurement set. To update L_{diff}, however, r must be evaluated over the complete range of the reflectance and incidence zenith angles and azimuth angles to perform the integrations as defined in (3). The updating of L_{diff}^{inc}, in particular, requires that r be evaluated at reflectance and incidence zenith angles defined for gaussian quadrature integration, necessary when accounting for the atmosphere-surface interaction. If the reflectance measurements L are made with an instrument like PARABOLA, the downward diffuse radiance.

L_{diff}^{inc} also is measured and can be directly inserted in (3) thus bypassing the process to compute it. Because of the hemispheric angular coverage of the measurements, the evaluation of r at the selected reflectance zenith angles and azimuth angles requires only the use of standard interpolation procedures. The evaluation of r over the full range of incidence zenith angle, however, can be accurately accomplished only if observations of a surface target are made at a number of different solar zenith angles. These multiple (distinct solar zenith angle) data sets then should be analyzed together so that the individual estimates of r at the different solar zenith angles using (4) or (5) can be introduced into (3) to compute L_{diff} which then is used in (4) in the, next iteration of the individual data sets. Depending on the number of sufficiently unique sun angle measurement sets, a linear or cubic splint technique generally is employed to interpolate or extrapolate the iterated estimates of r at the different solar zenith angles to gaussian quadrature incidence zenith angles for use in (3). If only a single sun angle measurement set is available, r is assumed to be independent of incidence zenith angle. The accuracy to which L_{diff} can be computed obviously depends on the accuracy to which the incidence zenith angle dependence of r can be estimated and thus directly affects the ultimate accuracy to which r can be retrieved.

Using (4) as expressed above, the iterated estimations of r generally tend to oscillate about the solution, normally resulting in a relatively slow convergence. The process can be made considerably more efficient simply by averaging the current iteration estimate of r from (4) with the previous iteration estimate to obtain a modified current iteration estimate of r which then is substituted in (3) and in computing L_{diff}^{inc}.

Approximate approach

A distinctly faster but less accurate retrieval algorithm can be derived by relaxing the mathematical and physical rigor described in (3) and making some approximations. Starting from (2), the expression for reflected radiance can be rewritten as

$$L(-\mu, \mu_0, \phi-\phi_0) = \pi^{-1} r(-\mu, \mu_0, \phi-\phi_0) [E_{dir}(\mu_0) + E''_{diff}(\mu_0)] + A(-\mu, \mu_0, \phi-\phi_0) \quad (6)$$

where E''_{diff} is the downward diffuse irradiance including all multiple reflections between the surface and atmosphere, and A is a residual term,

$$\Lambda(-\mu,\ \mu_0,\ \phi-\phi_0) = \pi^{-1}\int_0^1\int_0^{2\pi} r(-\mu, \mu', \phi-\phi')\, L_{diff}^{inc}(\mu', \mu_0, \phi'-\phi_0)\, \mu'\, d\mu'\, d\phi'$$

$$- \pi^{-1} r(-\mu, \mu_0, \phi-\phi_0) \int_0^1\int_0^{2\pi} L_{diff}^{inc}(\mu', \mu_0, \phi'-\phi_0)\, \mu'\, d\mu'\, d\phi'. \qquad (7)$$

Note that the integral in the last term in (7) is equal to E''_{diff}. The residual A can be small depending on the characteristics of r (little dependence on incidence and azimuth angles) or the amount of atmospheric opacity (small L_{diff}^{inc}). Now, if it is assumed that the surface behaves as a lambertian scatterer when considering multiple reflections between the surface and the atmosphere, then the total incident irradiance at the surface can be written as

$$E_{dir}(\mu_0) + E''_{diff}(\mu_0) = \frac{E_{dir}(\mu_0) + E_{diff}(\mu_0)}{1 - A\, S}. \qquad (8))$$

E_{diff} is the incident diffuse irradiance assuming no atmosphere-surface interaction (i.e., a black surface), A is the hemispherical reflectance (albedo) of the surface, and S is defined by

$$S = \pi^{-1} \int_0^1\int_0^{2\pi} \int_0^1\int_0^{2\pi} s(\mu', -\mu'', \phi'-\phi'')\, \mu'\, d\mu''\, d\phi''\, d\mu'\, d\phi' \qquad (9)$$

with s representing the atmospheric reflectance function for radiation scattered from the underside of the atmosphere. The surface BRF then can be expressed as

$$r(-\mu, \mu_0, \phi-\phi_0) = \frac{[L(-\mu, \mu_0, \phi-\phi_0) - \Lambda(-\mu, \mu_0, \phi-\phi_0)]\,[1 - AS]}{\pi^{-1}[E_{dir}(\mu_0) + E_{diff}(\mu_0)]} \qquad (10)$$

$$\cong \frac{L(-\mu, \mu_0, \phi-\phi_0)\,[1 - AS]}{\pi^{-1}[E_{dir}(\mu_0) + E_{diff}(\mu_0)]} \qquad (11)$$

when A is assumed small and is ignored. Expression (11) is similar to the estimate of r described by (5) but includes the contribution of E_{diff} and an approximation for the multiple reflections of radiation between the surface and atmosphere. With the directional hemispherical reflectance A defined as

$$A(\mu_0) = \pi^{-1} \int_0^1\int_0^{2\pi} r(-\mu, \mu_0, \phi-\phi_0)\, \mu\, d\mu\, d\phi, \qquad (12)$$

and integrating (11) in accordance with (12), the albedo A is given by

$$A = \frac{G}{1 + S G} \tag{13}$$

where

$$G = \frac{1}{[\,E_{dir}(\mu_0) + E_{diff}(\mu_0)\,]} \int_0^1 \int_0^{2\pi} L(-\mu, \mu_0, \phi-\phi_0)\, \mu \, d\mu \, d\phi \,. \tag{14}$$

G is the ratio of irradiance leaving the surface to the incident (black surface) irradiance. Knowing A from (13), r then can be evaluated using(11). "This retrieval scheme for r is one to two orders of magnitude faster than the more rigorous, iterative version described previously. Since this relaxed, non-iterative version dots not include any incidence angle dependence of r (such dependence being contained solely in the neglected parameter A), it generally will be less accurate than the rigorous version.

Ratioing approach

It is informative to compare r in (11) with the expression for the experimental directional reflectance factor, described earlier as the ratio of directionally reflected radiance from the surface to the nadir radiance from a reference target. Assuming that the reference target is ideally lambertian, the reflected radiance from the target can be expressed by (6), rewritten as

$$L_{ref}(\mu_0) = \pi^{-1} [\,E_{dir}(\mu_0) + E''_{diff}(\mu_0)\,] \tag{15}$$

where the BRF r is by definition unity for an ideal lambertian surface and A is zero. The ratioed radiance for the target Of interest then is

$$\frac{L(-\mu, \mu_0, \phi-\phi_0)}{L_{ref}(\mu_0)} = \frac{L(-\mu, \mu_0, \phi-\phi_0)}{\pi^{-1}\,[\,E_{dir}(\mu_0) + E''_{diff}(\mu_0)\,]}$$

$$= r(-\mu, \mu_0, \phi-\phi_0) + \frac{\pi\,\Delta(-\mu, \mu_0, \phi-\phi_0)}{[\,E_{dir}(\mu_0) + E''_{diff}(\mu_0)\,]} \,. \tag{16}$$

Note that(16) is almost the same expression as(10) and therefore essentiall y describes the relaxed algorithm when A is assumed to be negligible. If A is indeed negligible, interpreting the ratioed surface reflectance measurements as bidirectional reflectance factors results in a valid correction for atmospheric effects. Field measurements by Deering and Eck (1987), however, clearl y show that A can be quite substantial under hazy conditions, thereby reducing the accuracy of the dctcrmination of r by the ratioing tcchniquc.

It should bc noted that a conceptual difference exists bctwccn (1 O) and (16) because the reflection properties of the surface arc considered to bc lambcrtian in thc atmcwphcrc-surface multiple reflection process dcscribing the incident radiance in (1 O) whereas the true total incident radiance is used in (16). A comparison of computational results bct wccn the two sit uations, howcvcr, showed only insignificant differences for the various atmospheric conditions and surface types considcrcd in this study, indicating that a high dcgrcc of accuracy still is retained when using the lambcrtian approximation. Thus, (1 O) can bc used as an equivalent rcprcscntation

of (1 6).

MULTI-ANGLE RADIANCE DATA SETS

The rigorous and relaxed surface rcflcctancc rctrieval algorithms were applied to various sets of simulated multi-angle radiances, computcd for different types of dircctionally reflecting surfaces ovcrlain by an atmosphere containing acrosols. The bidirectional rcflcctancc factors describing the surface rcflcction propcrtics were derived from mcasurcmcnts, made under clear skies of 11 distinct types of natural surfaces in AVHRR wavelength bands 1 and 2 at 0.58-0.67 μm and 0.73- 1.1 pm, rcspcctivcly (Kimcs, 1983; Kimcs ct al., 1985a, b), providing 22 distinct BRF cases to bc analyzed in this study. The characteristics of the various BRF types arc listcd in Table 1. These cxpcrimcntal rcflcctancc factors, obtained by the ratioing technique, arc not the actual bidirectional rcflcctancc factors of the surface because of the impact of the A term effect discussed above and also bccausc of angular smoothing effects due to the finite (1 2°) field-of-view of the instrument. For the purposes of this study, however, it can bc assumed that the experimental rcflcction factors arc the true surface bidircctional rcflcctancc factors.

The mcasurcmcnts were made over the entire azimuth anglc range, starting from the principal plane and proceeding in 45° increments, and ovcr the zcnith anglc range from 0° to 75° in 15° increments for a total of 41 measurements pcr solar zcnith anglc. To guarantee reflection symmetry through the principal plane, the mirror-image radiance pairs through the principal planc were averaged, thus leaving a total of 26 indcpcndcnt data points pcr mcasurcmcnt set. The scalar zenith anglc covcragc varicd, depending on the surface type, but measurements were usual] y made at 3 or 4 different sun positions. Solar zenith angle covcragc for the complctc set of 11 surface types ranged bctwccn 23° to $2°. A 2-dimcnsional cubic splint intcrpolation scheme then was applied to these data sets to compute thc BRF at arbitrary incidcncc and rcflcction angles for usc in the radiative transfer procedure.

Three different sun geometries were investigated, defined by solar zenith angles of 25.6°, 45.9°, and 64.0° and an azimuth angle ϕ_0 of O°. The directional hemispherical reflectances for the 11 surface types in the two spectral bands and at the three selected sun angles were computed by integrating the BRF over view angle according to (12) and are displayed in the bar graph shown in Figs. 1a, b. They range from a low of 0.032 (soybeans, case 10 in band 1 at a sun angle of 45.90, to a high of 0.621 (irrigated wheat, case S in band 2 at a sun angle of 64.00). The corresponding BRF cases also have a wide variety of shapes, ranging from strong backward and forward scattering to little or no angular variability. For example, soil (case 1) exhibits strong backward scattering in band 1 which is highly dependent on sun angle, while a pine forest (case 7) exhibits moderate forward and backward scattering in band 1 for most sun angles. These two surface types represent the reflection variability extremes for the cases in Table 1 and arc used as examples in the subsequent retrieval analysis.

The atmospheric models used in the radiance simulations contain both Rayleigh and aerosol scat tering. The Rayleigh opacity was set to ().()49 for band 1 and 0.010 for band 2 with a standard atmospheric scale height. The optical properties of the aerosols were assumed to be identical in bands 1 and 2. The aerosol scattering was assumed to be Mic with a phase function described by an asymmetry parmctcrgof0.517, a single-scattering albedo ω of 1.0, and with a particle density scale height of 2 km. A number of different aerosol opacities τ were considered, ranging from 0.0 to 0.5.

Using the 22 surface BRF cases and the acrmxd-laden atmospheric models described above, simulated ground-level radiance data sets for a PARABOI,A-like instrument were computed using a coupled atnmspbcrc-surface radiative transfer code with view angles set at the same values as the experimental directional reflectances noted above. As a simplification, the simulated data sets do not include the effects of a finite view solid angle. If the retrieval is to be performed on a real data set, however, it is straightforward to include an integration over view solid angle in the described retrieval algorithms.

RETRIEVAL RESULTS

In this part of the retrieval study wc first test the accuracy of the iterative retrieval scheme described by expressions (3), (4) and (5). To achieve maximum accuracy in the retrieval process, a combined data set was used which included the reflection measurements at all three of the noted solar zenith angles (25.6°, 45.9°, and 64.00). Use of the three sun angle sets together instead of individually allows a more accurate computation of L_{diff} as expressed by (3) since the sun angle dependence of r and L_{diff}^{inc} more readily can be taken into account. For the heavily laden aerosol condition ($\tau = 0.5$), the retrieved directional reflectance factors for the 11 BRF cases in band 1 are displayed in Fig. 2, expressed in terms of the fractional deviation δ at each sun position.

The fractional deviation δ for a given BRF type is defined as

$$\delta(\mu_0) = \frac{1}{N}\sum_{ij}\left|\frac{r(\mu_i, \mu_0, \phi_j - \phi_0) \cdot r_0(\mu_i, \mu_0, \phi_j - \phi_0)}{A(\mu_0)}\right| \qquad (17)$$

where r and *r.* are the retrieved and true directional reflectance factors respectively, *A is* the true directional hemispherical albedo, and N is the number of unique measurements (26 for the described data sets) at the given sun position. Similar results to those of band 1 were obtained for the BRF cases of band 2, as was true for all aspects of this study. Therefore, in the interest of brevity, only the results from band 1 are illustrated in this paper.

Although the irrigated wheat BRF (case 5) at 64.0° solar zenith angle in band 1 shows a fractional deviation as high as 0.096, the average fractional deviation for the 22 BRF cases is under 0.03. Research into the cause of the much larger than average deviations associated with cases 1, 5,6 and 7 in Fig. 2 showed that the BRF variation with incidence angle for these cases was strong and the 3 sun angle data sets used in the retrievals were not sufficient in number to totally account for such a wide range of variation. Note also that from (17) the average error in the retrieved BRF is given by the product of $\delta(\mu_0)$and $A(\mu_0)$. Thus, for case 5 at 64.0° solar zenith angle the average BRF error is only 0.096 x 0.090= 0.0086.

The directional hemispherical reflectances computed from the retrieved bidirectional reflectance factors for the 11 cases in band 1 are shown in Fig 3 as a percent difference from the correct values of Fig. 1, that is, 100% x (retrieved - true) / true). The largest errors in the hemispherical reflectances reach about 8% but the average errors for all 22 BRF cases is just over 2%. Retrievals were also done on the data sets where the aerosol loading was not so great and the results show the same trends as the heavy loading situation but with a steady improvement in accuracy with decreasing aerosol opacity. For the data sets with an opacity of 0.1 there is about a factor of two improvement in retrieval accuracy over those data sets with an opacity of 0.5, for both the individual BRF cases and the directional hemispherical reflectances.

To determine how sensitive the retrieval results are to sun angle coverage of the measurements, retrievals were performed on the same data sets as above but used only a single sun angle data set per retrieval trial. Thus, three independent trials were run at each of the specified sun angles. This method implies that the μ' dependence in the integral of (3) is replaced by the constant μ_0 of the particular sun geometry being considered in the retrieval process, but that the azimuthal angle dependence $\phi-\phi'$ for that sun geometry is still maintained within the integral. This is, therefore, an intermediate case between that of the rigorous retrieval algorithm which considers the full μ', $\phi-\phi'$ dependence of r by using multi-angle sun geometry data sets and the relaxed algorithm which replaces the μ', $\phi-\phi'$ dependence with the particular $\mu_0,\phi-\phi_0$ of a single-angle sun geometry data set. Fig. 4 shows the retrieval results in band 1, expressed as fractional deviations, using this intermediate retrieval algorithm on those data sets produced with an aerosol opacity of 0.5. The corresponding results for the same data sets but using the relaxed algorithm described by (11) are displayed in Fig. 5. Sample comparisons in accuracy between the various algorithms of the retrieved directional reflectance factors in the principal plane are illustrated in Figs. 6, 7 and 8 for the individual cases of the plowed field, irrigated wheat, and the pine forest, respectively, at a solar zenith angle of 64.0°. A significant reduction in accuracy is evident when the results from either of these two alternative algorithms are compared to those from the rigorous algorithm. This accuracy degradation also applies to the retrieved directional hemispherical reflectances, displayed in Figs. 9 and 10, when using either the intermediate or relaxed algorithm. For those data sets produced with progressively smaller aerosol opacities, the retrieval results followed the same trends as those illustrated for the data sets with an opacity of 0.5 but with systematically increasing accuracy. The retrieval results for the data sets with an aerosol opacity of 0.1, for example, were three to four times more accurate than the results in Figs. 5 through 10.

From these trials it can be concluded that retrievals using combined multi-angle sun geometry data sets produce results with greater accuracy than retrievals using only a single sun angle data set. In turn, when a single sun angle data set is processed, the intermediate retrieval algorithm generally is more accurate than the relaxed algorithm. These conclusions are particularly true for those BRF cases which have a strong dependence on both solar zenith angle and solar azimuth angle, a good example being, that of soil as displayed in Fig. 6. When the solar angle dependence is less extreme, as in the case of the pine forest BRF case shown in Fig. 8 which nevertheless has a significant view angle dependence, the retrieval results from the various algorithm versions described here tend to be more similar to each other.

The trials also showed that the amount of atmospheric opacity can strongly influence the accuracy of the retrieval results, depending on the version of the algorithm used. Fig. 11 shows a summary of the retrieval tests for both the rigorous and relaxed algorithms, illustrating the dependence of the case-averaged fractional deviation δ on the amount of aerosol opacity. The corresponding results from the intermediate algorithm are not shown to avoid clutter but they tend to fall in the gap between those from the other two algorithms. For no aerosol the case-averaged/5 is about 0.003, duc to computational errors accrued during the removal of the effects of the Rayleigh opacity. When the aerosol opacity is on the order of 0.1 or less, both the rigorous and intermediate algorithms have essentially the same accuracy and the relaxed algorithm only a little lcss accuracy. Thus, the ratioing procedure, applied to field measurements taken under light aerosol loading, (in effect, an application of the relaxed algorithm) results in atmospherically corrected experimental reflectance factors which arc reasonable representations of the true surface bidirectional reflectance factors. For those measurements, however, made when the atmospheric opacity is substantial (O. 3 and greater), the accuracy of the atmospheric correction process can be severely compromised if the ratioing technique is employed. Under these conditions the intermediate algorithm should be used if the measurement set include only onc sun angle. When measurements at more than one sun angle arc available, the more rigorous iterative retrieval algorithm is preferred.

It should be emphasized that multi-angle sun geometry data sets will generall y have different aerosol conditions associated with each sun angle set. This may occur because the aerosol amount changed during the course of a day's worth of measurements or else data sets from different days arc combined. This presents no problem to the usc of the rigorous algorithm since each particular sun, angle data subset of the combined data set is processed using either an atmospheric model appropriate for the atmospheric conditions when the measurements were taken or else using the actual measurements of the downward diffuse radiance.

DISCUSSION

The retrieval trials described above show that BRF accuracies of 3% or better can be achieved when all other factors arc strictly controlled. In particular it was assumed that the atmospheric conditions were precisely known and therefore did not compromise the accuracy of the retrieval results. If ancillary atmospheric measurements arc taken in the same time period as the surface reflectance measurements, they typically include only sun photometry to determine the spectral aerosol opacity. Generally no other kinds of measurements are made from which to obtain additional aerosol information such as spectral single scattering albedos and phase functions.

The impact of uncertainties in the atmospheric parameters on surface BRF retrieval is illustrated in Figs. 12 and 13. Fig. 12 shows the fractional deviation δ assuming the same retrieval conditions as those that produced Fig. 2 except that an aerosol single scattering albedo ω of 0.9 was used instead of 1.0. Note the strong, systematic solar zenith angle dependence of δ, averaging more than 0.13 at 64.0° and receding to less than 0.06 at 25.6°. The corresponding directional hemispherical reflectances show a similar trend with an average percent difference of more than 11% at solar zenith angle of 64.0° and about 5% at 25.6°. Fig. 13 shows a similar trend when, again, the correct atmospheric conditions were assumed in the retrieval except that an aerosol phase function asymmetry parameter g of 0.714 was used instead of 0.517. Again, the increase in δ with solar zenith angle is evident, the average ranging from about 0.08 at 64.0° down to about 0.04 at 25.6°. The corresponding directional hemispherical reflectances are systematically smaller than the correct values with the average percent difference being almost -9% at solar zenith angle of 64.0° and about -3% at 25.6°.

A useful field data set which can help validate the aerosol model used in the surface retrieval is measurements of the downward diffuse sky radiance in a number of different directions. The value of an instrument like PARABOLA is its ability to measure diffuse sky radiance over most of the upward-looking hemisphere during the course of measuring the surface reflected radiance. When a subsequent surface retrieval is done using a particular aerosol model, it is straightforward to compute the associated downward radiances to which the measured sky radiance values can be compared. Fig. 14 shows such a comparison of downward diffuse radiance in the principal plane for the three aerosol models previously considered, namely the correct model (ω = 1.0, g = 0.517), and its two variations (ω = 0.9, g = 0.517) and (ω = 1.0, g = 0.714), all with an aerosol opacity of 0.5. The radiances for surface BRF case 1 (plowed field) at solar zenith angle 25.6° is illustrated but similar radiances at the same solar zenith angle are obtained for the other surface types. It is clear that the differences in the downward diffuse radiance predicted for the two variant aerosol models from that of the correct model directly account for the increased BRF retrieval deviations of Figs. 12 and 13 as compared to Fig.2. This problem of needing to know the atmospheric properties as a necessary condition for accurate surface reflectance retrievals can be completely bypassed, however, by making use of the measured downward diffuse radiances directly in the rigorous retrieval algorithm, as described earlier.

The only other major factor affecting the accuracy of the surface retrieval is the quality of the radiometric calibration of the instrument. Even if both the upward reflected surface radiance L and the incident diffuse radiance L_{diff}^{inc} are simultaneously measured by the same instrument, it can be seen from expressions (4) and (1 O) that the bidirectional reflectance factors, retrieved by either the rigorous or relaxed forms of the algorithm, are directly affected by errors in the radiometric calibration. This is due to the fact that the direct irradiance E_{dir} is normally determined by means of another instrument such as a sun photometer. However, the ratioing technique, described by expression (16), is completely insensitive to any radiometric calibration errors because both the direct and diffuse radiance are effectively measured by the same instrument by means of the reference target. Rewriting (16),

$$r(-\mu,\mu_0,\ \phi-\phi_0) = \frac{L(-\mu,\mu_0,\phi-\phi_0) - \Delta(-\mu,\mu_0,\ \phi-\phi_0)}{L_{ref}(\mu_0)} \qquad (17)$$

a genera form for r with no approximations. If downward diffuse radiance measurements L_{diff}^{inc} are also ma(? in addition to L and L_{ref}, then A, described by (7), has the same calibration accuracy as L and L_{ref} and the evaluation of r via (17) will be insensitive to calibration errors. If the reference target is onl y approximately an ideal lambertian reflector, L_{ref} in (17) can be replaced by L''_{ref} where

$$L''_{ref}(\mu_0) = \frac{L_{ref}(-\mu,\mu_0,\phi-\phi_0)}{r_{ref}(-\mu,\mu_0,\phi-\phi_0)} = \pi^{-1} E_{dir}(\mu_0)$$

$$+ \frac{\pi^{-1}}{r_{ref}(-\mu,\mu_0,\phi-\phi_0)} \int_0^1\int_0^{2\pi} r_{ref}(-\mu,\mu',\phi-\phi')\, L_{diff}^{inc}(\mu',\mu_0,\phi'-\phi_0)\ \mu'\, d\mu'\, d\phi'$$

$$\cong \pi^{-1} E_{dir}(\mu_0) + \pi^{-1} \int_0^1\int_0^{2\pi} L_{diff}^{inc}(\mu',\mu_0,\phi'-\phi_0)\ \mu'\, d\mu'\, d\phi'$$

$$= \pi^{-1}[\,E_{dir}(\mu_0) + E''_{diff}(\mu_0)\,] \qquad (18)$$

and r_{ref} is the known BRF of the reference target. Expressions (7), (17) and (18) then become the preferred algorithm equations instead of (3) and (4) for obtaining the highest accuracy in retrieved surface reflectance. Multi-directional measurements of L_{diff}^{inc} thus serves three major purposes: 1) they eliminate the need to know the atmospheric characteristics of the atmosphere; 2) they eliminate the sensitivity of the retrieved surface reflectances to instrument radiometric calibration uncertainties, when used in conjunction with reference target measurements; and (3) they eliminate the need to compute L_{diff}^{inc} using complicated, time-consuming, multiple scattering radiative transfer routines. Measurements of L_{diff}^{inc} have an additional intrinsic accuracy in that they correctly account for the multiple reflections of radiation between the atmosphere and terrain surrounding the target without the need to assume that the terrain surface reflectance properties are the same as those of the target. This ability to bypass detailed knowledge of the atmosphere, the surrounding terrain, and the instrument calibration and still be able to perform an accurate surface BRF retrieval should be sufficient incentive for making multi-directional downward diffuse radiance measurements an integral part of surface BRF field work.

Once the surface BRF is accurately retrieved it then is possible to analyze the downward diffuse measurements with regard to retrieving aerosol optical properties. Fig 14 indicates that the dependence of diffuse radiance with view zenith angle is strongly dependent on the properties of the aerosols, particularly the phase function asymmetry which, in turn, depends on the particle size distribution. For a solar zenith angle of 25.6° the aerosol phase function which is more strongly forward scattering (g=0.7 14) produces an aureole about the corresponding view zenith angle which is essentially absent from the other, less forward scattering, aerosol phase function (g=0.5 14). Inversion techniques applied to aureole measurements for the retrieval of aerosol size distributions have been investigated previously, (e.g. Green et al.(1971); Deepak (1977)). However, the analysis usually is limited to a relatively small angular range (about 20°) from the position of the sun where single scattering dominates. If the diffuse radiance measurements covering essentially the complete upward hemisphere are to be correctly analyzed, then the additional effects of multiple scattering, surface-atmosphere reflections, and finite instrumental field-of-view must be adequately addressed.

A successful retrieval of the aerosol single scattering albedo using diffuse radiance measurements is highly dependent on the quality of the radiometric calibration of the instrument. A comparison of the diffuse radiance curves in Fig. 14 with $\omega = 1.0$ and 0.9 shows basically a scaling difference between them, an effect which could easily be masked by instrumental calibration errors or uncertainties. When the aerosol opacity is smaller than 0.5, the value illustrated in Fig. 14, this difference becomes correspondingl y smaller and more difficult to discern. Nevertheless, in spite of the problems in the interpretation of multi-directional downward diffuse radiance measurements, these data sets contain information about aerosol properties that is difficult to obtain otherwise.

SUMMARY

It is possible to retrieve accurate bidirectional reflectance factors using multi-directional measurements of surface reflected radiance provided certain observational and measurement strategies are employed. Simulated ground level surface reflectance measurements, uniformly gridded in view angle over the whole downward-looking hemisphere, were used to show that the accuracy of the retrieved surface properties (bidirectional reflectance factors and directional hemispherical reflectance) was greatly improved if these gridded surface reflectance measurement sets were available over a wide range of solar zenith angles and were used together in the retrieval algorithm. When a gridded set at a single sun position was analyzed separately, the accuracy of the resulting surface property retrieval was diminished to an extent depending on how sensitive the BRF was to the incident angle geometry; high sensitivity resulted in larger inaccuracies.

A rigorous retrieval algorithm involving iteration was described which preserved the full extent of the angular geometry of the surface BRF in the radiative transfer process and included all atmosphere-surface reflection effects. A relaxed version of the algorithm was also derived, having the virtues of speed and greater simplicity, but confining approximations which allowed the processing of gridded measurement sets at only a single solar zenith angle. It produced retrieval results which, in general, were less accurate than those from the rigorous algorithm when also processing only a single sun position measurement set. The technique of ratioing the surface reflectance measurements of a target with unknown surface properties to those from a reference target with ideal or near-ideal lambertian reflectance properties was shown to be essentially the same algorithm as the relaxed algorithm. The difference between them is that the relaxed algorithm must compute the diffuse and direct irradiances whereas the ratioing technique essentially measures them.

This study found that a key measurement set, necessary for both accurate and efficient surface property retrievals, is that containing ground level multi-directional downward diffuse radiances, gridded over the upward-looking hemisphere in a similar fashion to the surface reflectance measurements. These measurements obviate the need for detailed knowledge of the atmospheric optical properties and the surrounding terrain reflection properties, both necessary inputs to the computation of downward diffuse radiances, and also the need to perform any detailed radiative transfer computations. In addition, if these gridded radiance measurement sets, both upward and downward directed, are complemented by reflectance measurements from a known,

near-lambcrtian rcfcrcncc target, then the surface propcrty retrievals arc also insensitive to instrument radiomctric calibration errors.

The author would like to express his appreciation to Eric Danielson for his assistance in the graphical aspects of this work. This research was carried out by the Jet Propulsion Laboratory, California Institutc of Technology, under contract with the National Aeronautics and Space Administration.

REFERENCES

Charney, J., Quirk, W. J., Chow, S., and Kornfield, J. (1977), A comparative study of the effects of albedo change on drought in semi-arid regions, *J. Atmos. Sci., 34:1366-1385.*

Deepak, A. (1977), *Methods in Atmospheric Remote Sounding* (A. Deepak, ed.) Academic Press, pp. 265-295.

Deering, D.W., and Leone, P. (1986), Sphere scanning radiometer for rapid directional measurements of sky and ground radiance, *Remote Sens. Environ. 19:1-24.*

Deering, D. W., and Eck, T.F. (1987), Atmospheric optical depth effects on angular anisotropy of plant canopy reflectance, *Int. J. Remote Sensing, 8:893-916.*

Dickinson, R.E. (1981), Land surface processes and climate-surface albedos and energy balance, *Adv. Geophys.*, 25:305-353.

Dickinson, R. E., Pinty, B., and Verstraete, M.M. (1990), Relating surface albedos in GCM to remotely sensed data, *Agriculture and Forest Meteorology, 52:109-131.*

Green, A. E. S., Deepak, 'A., and Lipofsky, B.J. (1971), Interpretation of the sun's aureole based on atmospheric aerosol models, *Appl. Opt., 10:1263.*

Kimes, D.S. (1983), Dynamics of directional reflectance factor distributions for vegetation canopies, *Appl. Opt., 22:1364-1372.*

Kimes, D. S., Newcomb, W.W., Nelson, R. F., and Schutt, J. Il. (1985a) Directional reflectance distributions of a hardwood and pine forest canopy, *IEEE Trans. Geosci. Remote Sens.,* GE-24: 281-293.

Kimes, D. S., Newcomb, W.W., Tucker, C. J., Zonneveld, 1. S., Van Wijngaarden, W., deLeeuw, J., and Epema, G.F. (1985b), Directional reflectance factor distributions for cover types of Northern Africa in NOAA 7/8 AVHRR Bands 1 and 2, *Remote Sens. Environment, 18:1-19.*

Mintz, Y. (1984), *The Global Climate* (J.T. Houghton, ed.), Cambridge University Press, Cambridge, London, New York, pp. 79-105.

Nicodemus, F. E., Richmond, J. C., Hsia, J. J., Ginsberg, I. W., and Limperis, T. (1 977), *Geometrical Considerations and Nomenclature for Reflectance, NBS* Monograph 160, National Bureau of Standards, U.S. Department of Commerce, Washington, D.C.

Pinty, B. and Verstraete, M.M. (1991), Extracting information on surface properties from bidirectional reflectance measurements, *J. Geophys. Res.*, 96:2865-2874.

Pinty, B. and Verstraete, M.M. (1992), On the design and validation of surface bidirectional reflectance and albedo models, *Remote Sens. Environ., 41:155-167.*

Starks, P. J., Norman, J. M., Blad, B.L., Walter-shea, E. A., and Walthall, C. L. (1991), Estimation of shortwave hemispherical reflectance (albedo) from bidirectionally reflected radiance data, *Remote Sens. Environ. 38:123-134.*

Table 1. Surface BRF Characteristics

Case	Cover Type	Location	Height (cm)	Coverage (%)
1	Plowed field	Tunisia, Africa		
2	Grassland	Tunisia, Africa	<3	<5
3	Steppe grass	Tunisia, Africa	38	18
4	Hard wheat	Tunisia, Africa	46	11
5	Irrigated wheat	Tunisia, Africa	76	70
6	Hardwood forest	Beltsville, Maryland	1100	75
7	Pine forest	Beltsville, Maryland	2200	79
8	Lawn grass	Beltsville, Maryland	14	97
9	Corn	Beltsville, Maryland	33	25
10	Soybeans	Beltsville, Maryland	77	90
11	orchard grass	Beltsville, Maryland	22	50

FIGURE CAPTIONS

Figure 1a. Histogram of directional hemispherical reflectance (albedo) in band 1 for the surface BRF cases listed in Table 1. The reflectances for three different solar zenith angles arc displayed for each case.

Fig.1b. Same as Fig. 1a except reflectances arc for band 2.

Figure 2. Retrieval of BRF in band 1 expressed as average fractional deviation (see text) using the rigorous, iterative algorithm and the combined reflectance data sets at the three solar zenith angles.

Figure 3. Percent difference in directional hemispherical reflectances in band 1 computed from retrieved bidirectional reflectance factors using the rigorous algorithm.

Figure 4. Retrieval of BRF in band 1 using the intermediate algorithm independently on each of the reflectance data sets at the three solar zenith angles.

Figure 5. Retrieval of BRF in band 1 using the relaxed, non-iterative algorithm independently on each of the reflectance data sets at the three solar zenith angles.

Figure 6. Retrieved BRF in band 1 in the principal plane for case 1 (plowed field) using the rigorous (triangles), intermediate (squares) and relaxed (stars) algorithms. For comparison the correct BRF is also shown (diamonds)

Figure 7. Same as Fig.6 but for case 5 (irrigated wheat).

Figure 8. Same as Fig.6 but for case 7 (pinewood forest).

Figure 9. Percent difference in directional hemispherical reflectances in band 1 computed from retrieved bidirectional reflectance factors using the intermediate algorithm.

Figure 10. Percent difference in directional hemispherical reflectances in band 1 computed from retrieved bidirectional reflectance factors using the relaxed algorithm.

Fig 11. Retrieved BRF fractional deviation, averaged over the 22 cases, as a function of aerosol opacity. Both the rigorous (solid lines) and relaxed algorithm (dashed lines) results arc shown for the three solar zenith angles (64.0°, diamonds; 45.9°, triangles; 25.6°, squares).

Fig. 12. Retrieval of BRF in band 1 using the rigorous algorithm, the combined reflectance data sets at the three solar zenith angles, and a modified aerosol mode] in which $\omega = 0.9$ instead of 1.0.

Fig. 13. Retrieval of BRF in band 1 using the rigorous algorithm, the combined reflectance data

sets at the three solar zenith angles, and a modified aerosol model in which $g = 0.714$ instead of 0.517.

Fig. 14. Downward diffuse radiance in the principal plane for BRF case 1 (plowed field) and a solar zenith angle of 25.6°. The radiance is ratioed to the normal irradiance at the top of the atmosphere. The nominal aerosol model is shown (diamonds) in addition to the two variant models described in the text ($\omega = 0.9$, triangles; $g = 0.714$, squares).

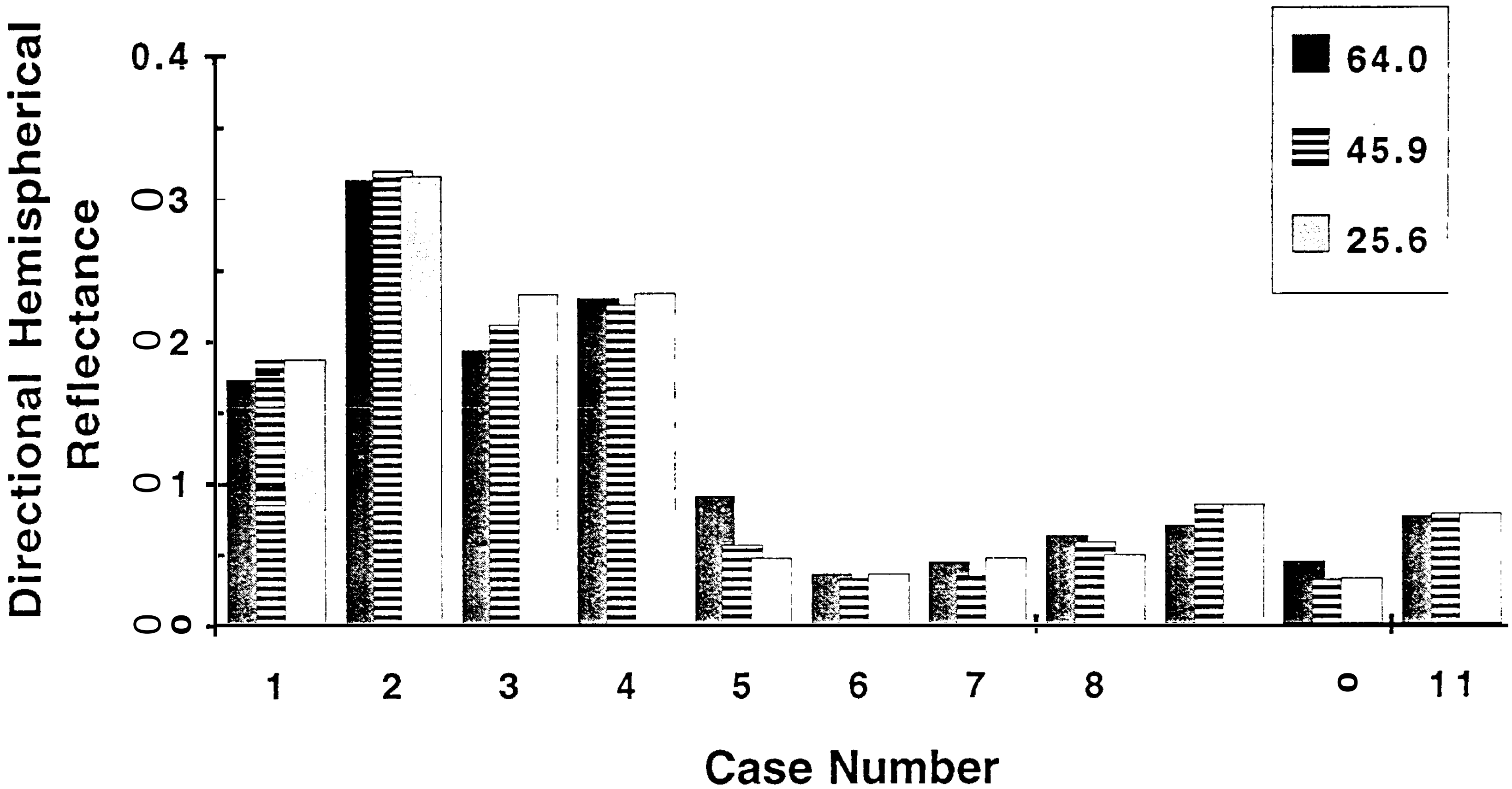

Directional Hemispherical Reflectance
0.4
0 3
0 2
0 1
0 0
64.0
45.9
25.6
1
2
3
4
5
6
7
8
o
11
Case Number

a

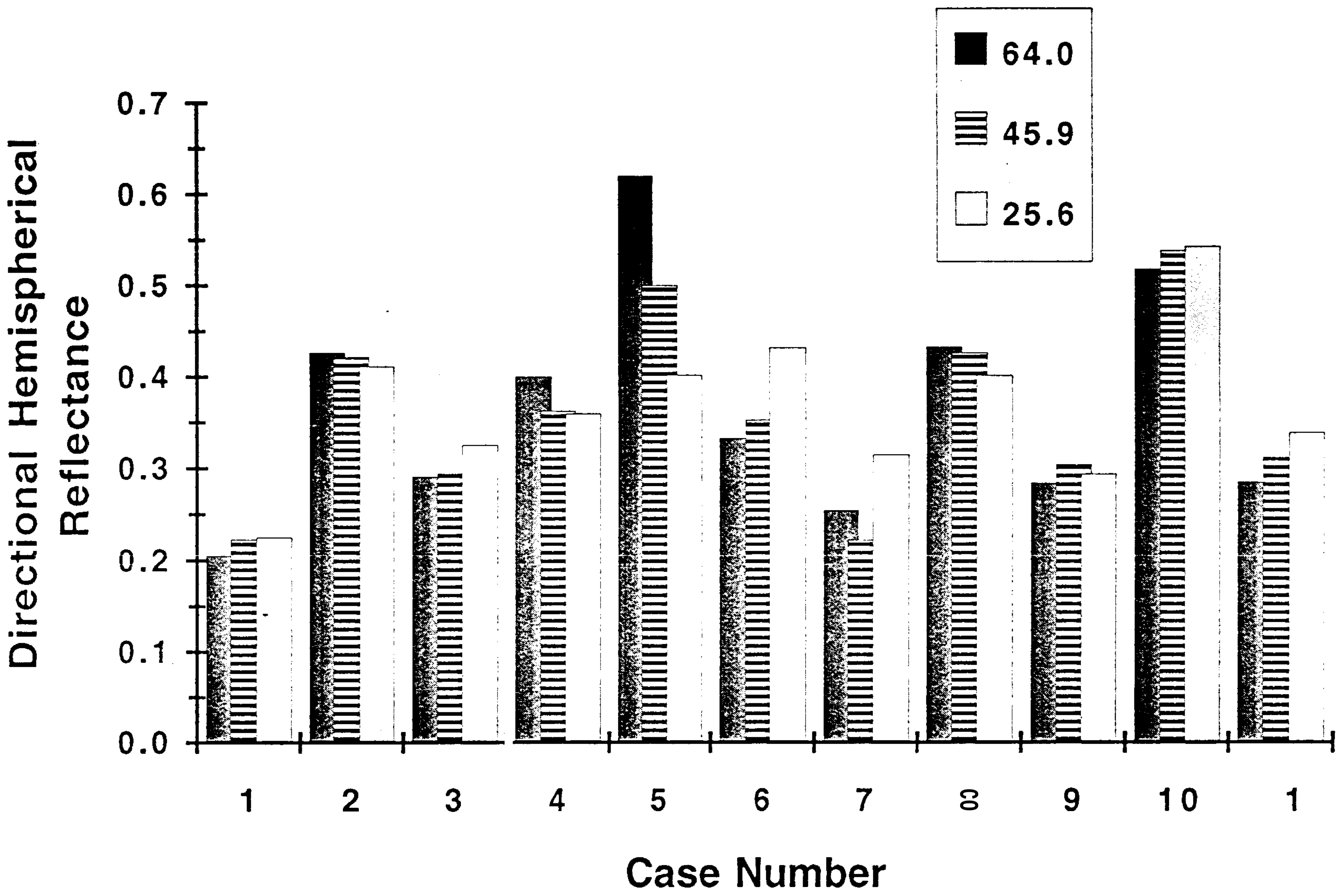
64.0
45.9
25.6
Directional Hemispherical Reflectance
0.7
0.6
0.5
0.4
0.3
0.2
0.1
0.0
1
2
3
4
5
6
7
8
9
10
1
Case Number

Figure 1b

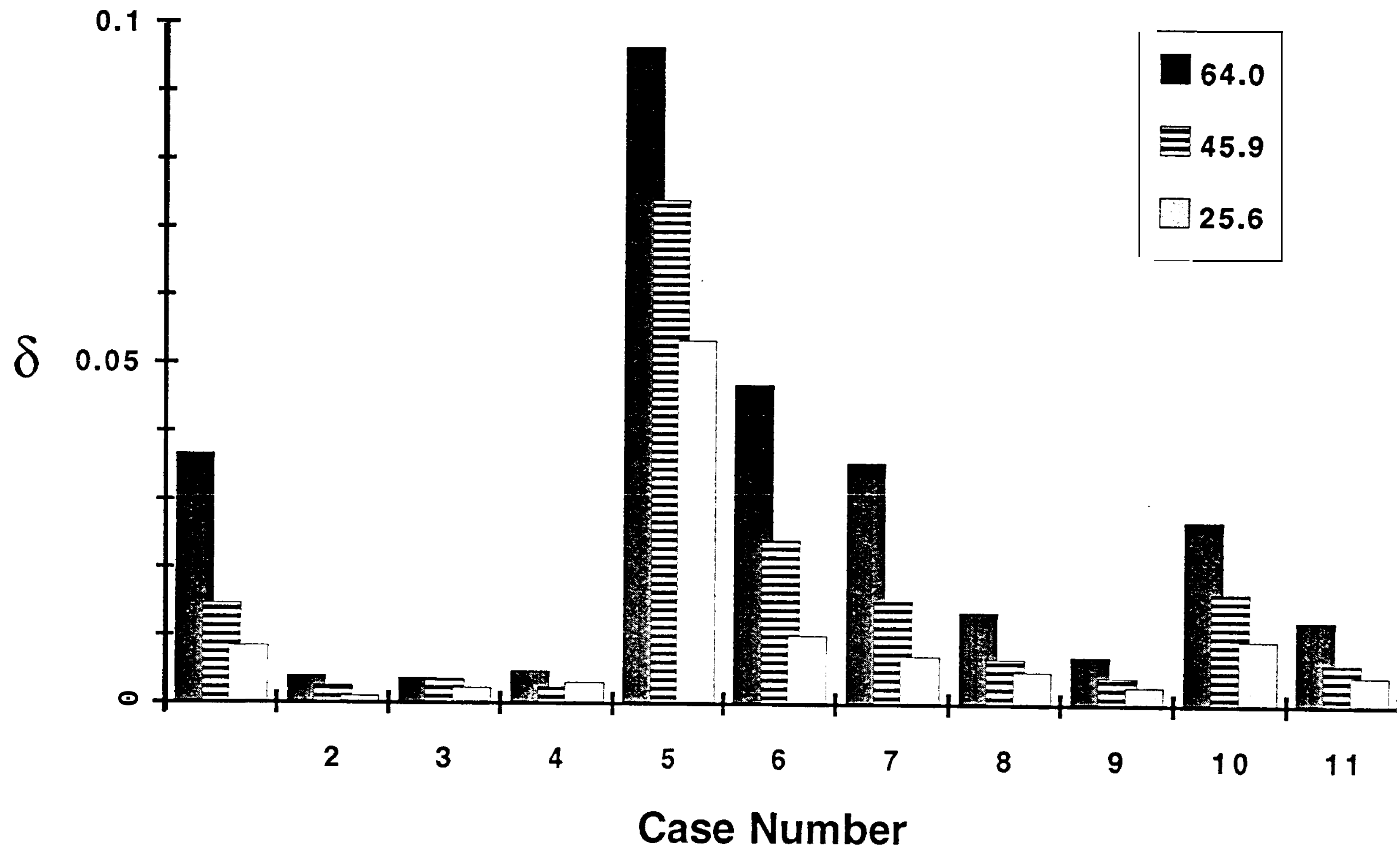

Figure 2

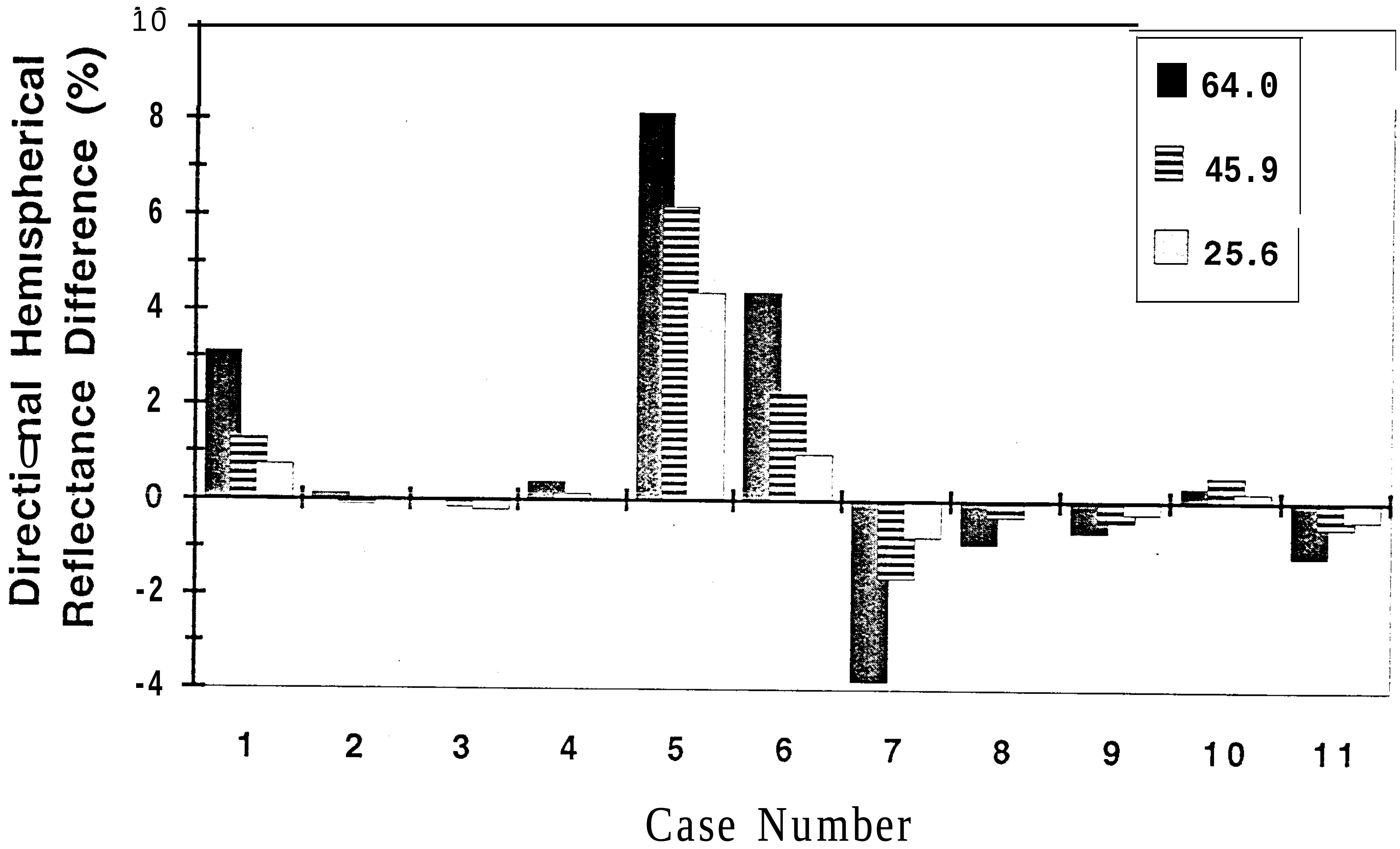
Directional Hemispherical
Reflectance Difference (%)
10
8
6
4
2
0
-2
-4
64.0
45.9
25.6
1
2
3
4
5
6
7
8
9
10
11
Case Number

Figure 3

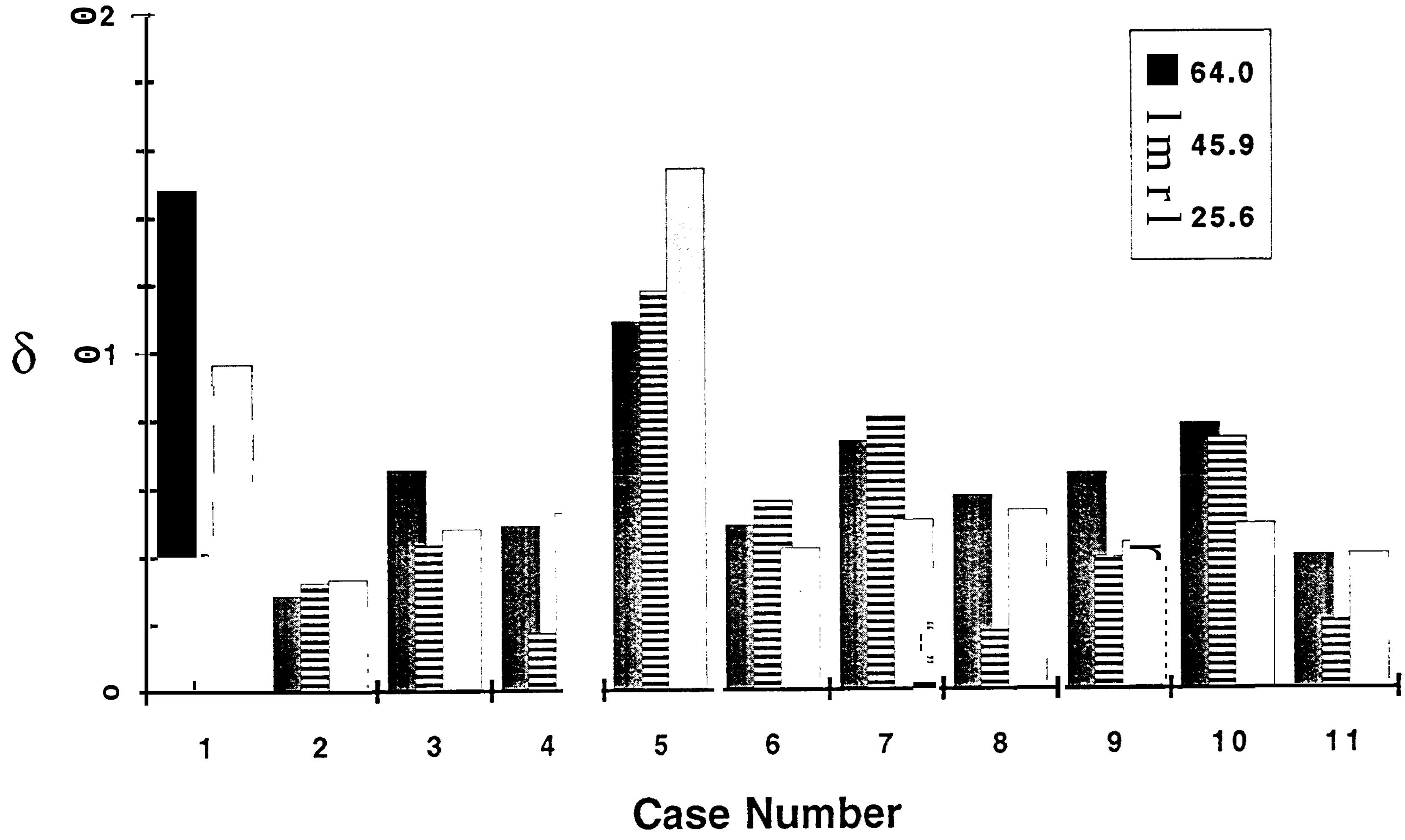

Figure

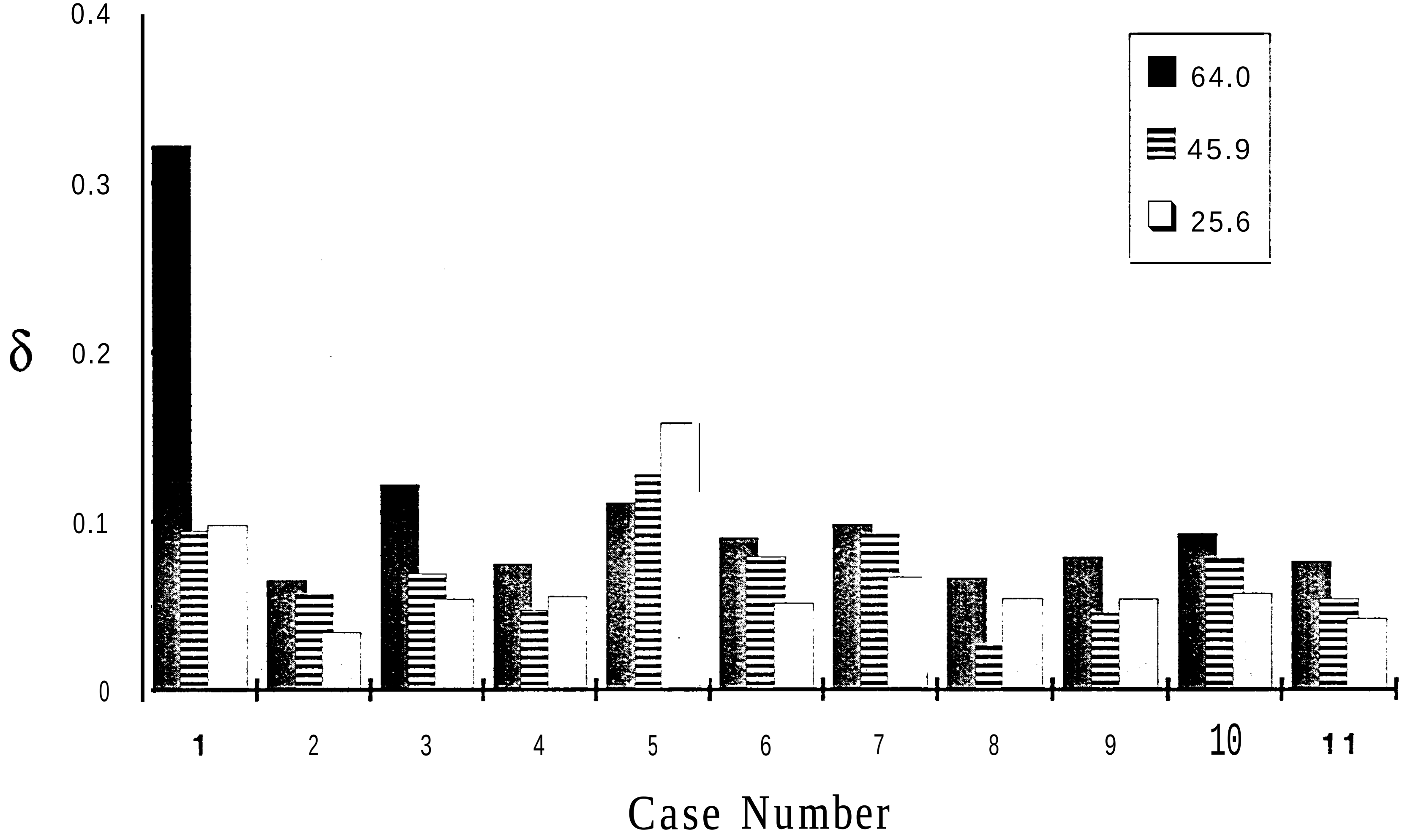

Figure 5

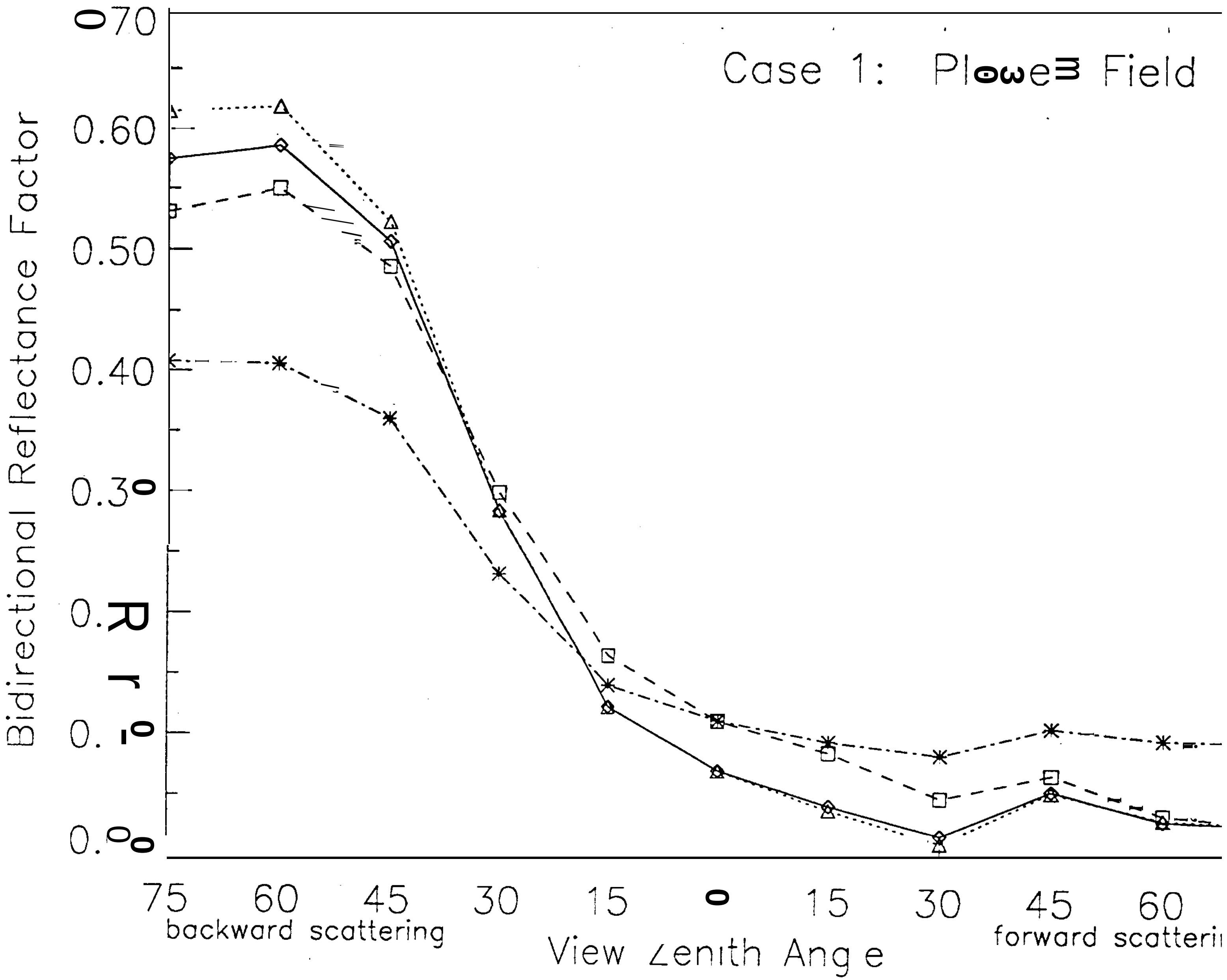

Case 1: Plowed Field
Bidirectional Reflectance Factor
0.70
0.60
0.50
0.40
0.30
0.00
75
60
45
30
15
0
15
30
45
60
backward scattering
forward scatteri
View Zenith Angle

Figure 6

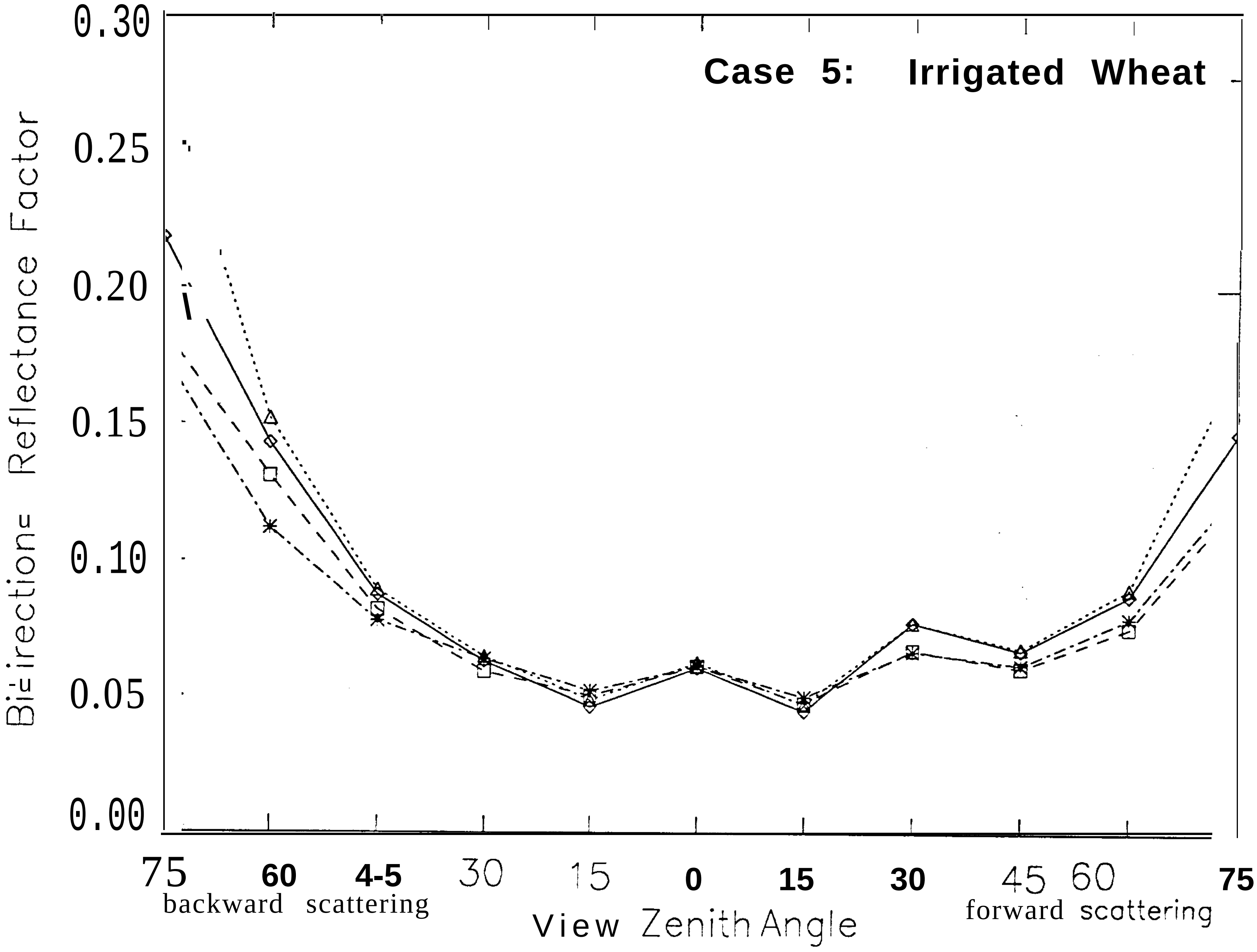
Case 5: Irrigated Wheat
Bidirectional Reflectance Factor
0.30
0.25
0.20
0.15
0.10
0.05
0.00
75 60 4-5 30 15 0 15 30 45 60 75
backward scattering
forward scattering
View Zenith Angle

Figure 7

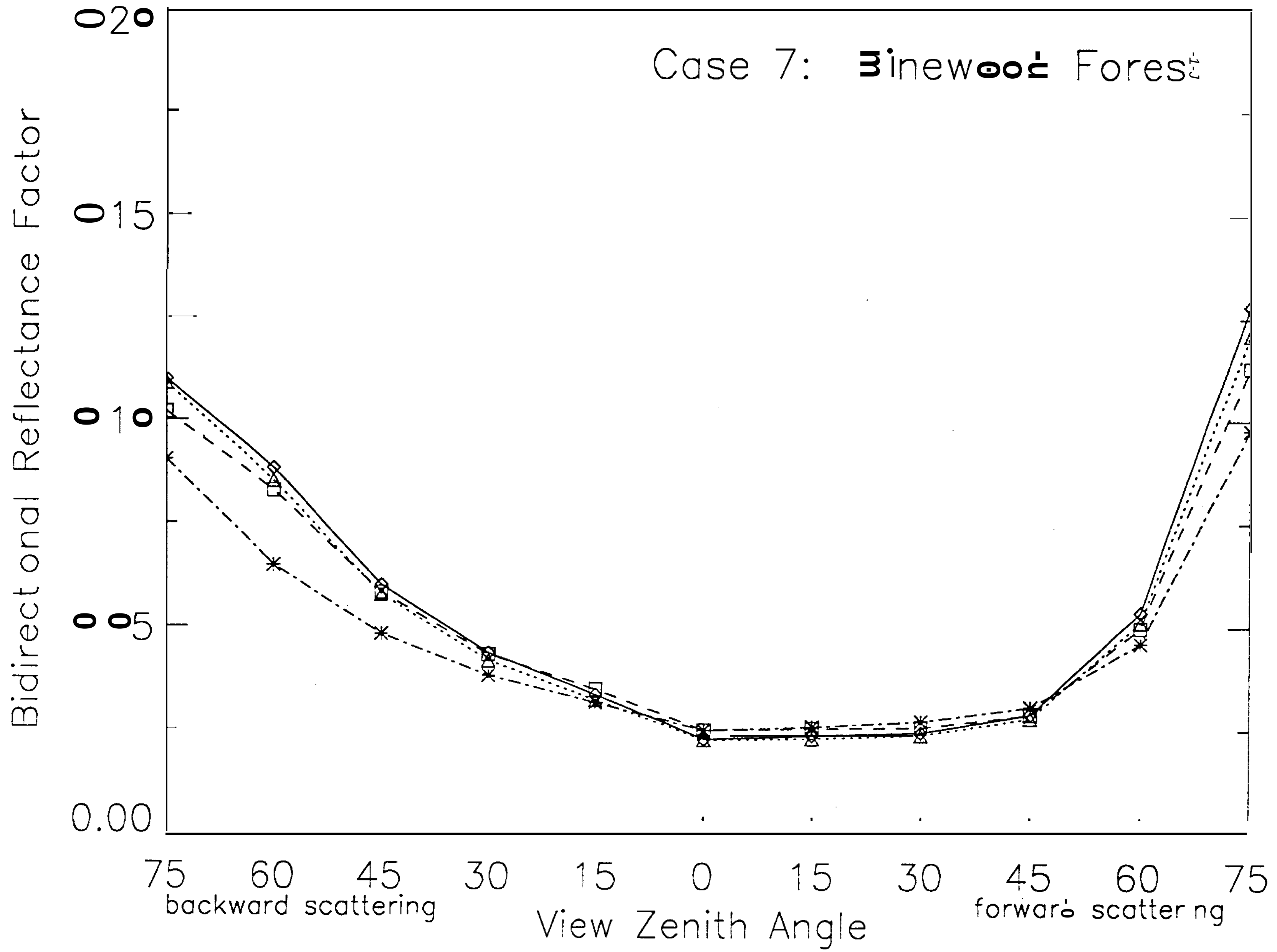
Case 7: Pinewood Forest
Bidirectional Reflectance Factor
0.20
0.15
0.10
0.05
0.00
75
60
45
30
15
0
15
30
45
60
75
backward scattering
View Zenith Angle
forward scattering

Figure 8

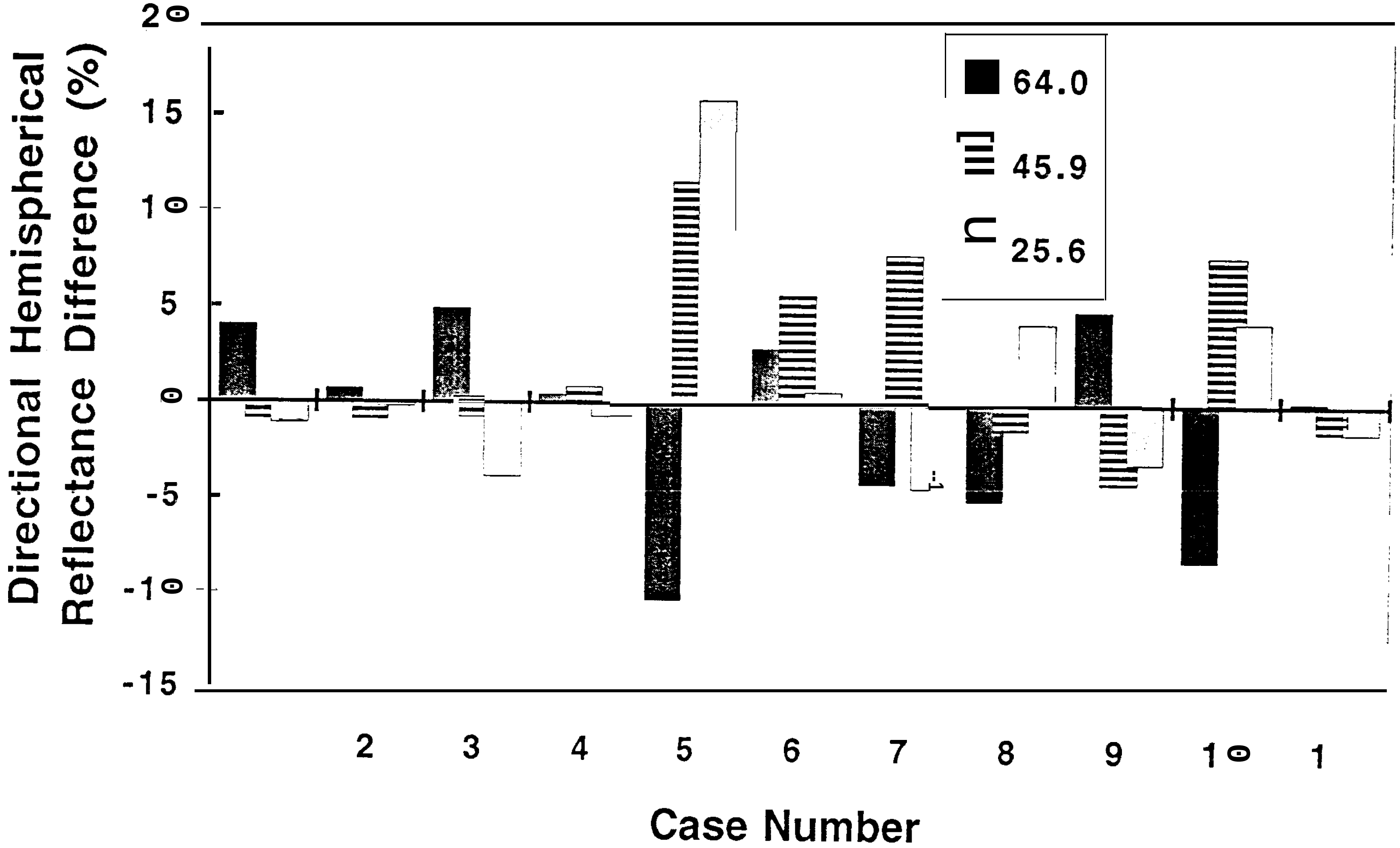

Directional Hemispherical Reflectance Difference (%)
20
15
10
5
0
-5
-10
-15
64.0
45.9
25.6
2
3
4
5
6
7
8
9
10
1
Case Number

Figure 9

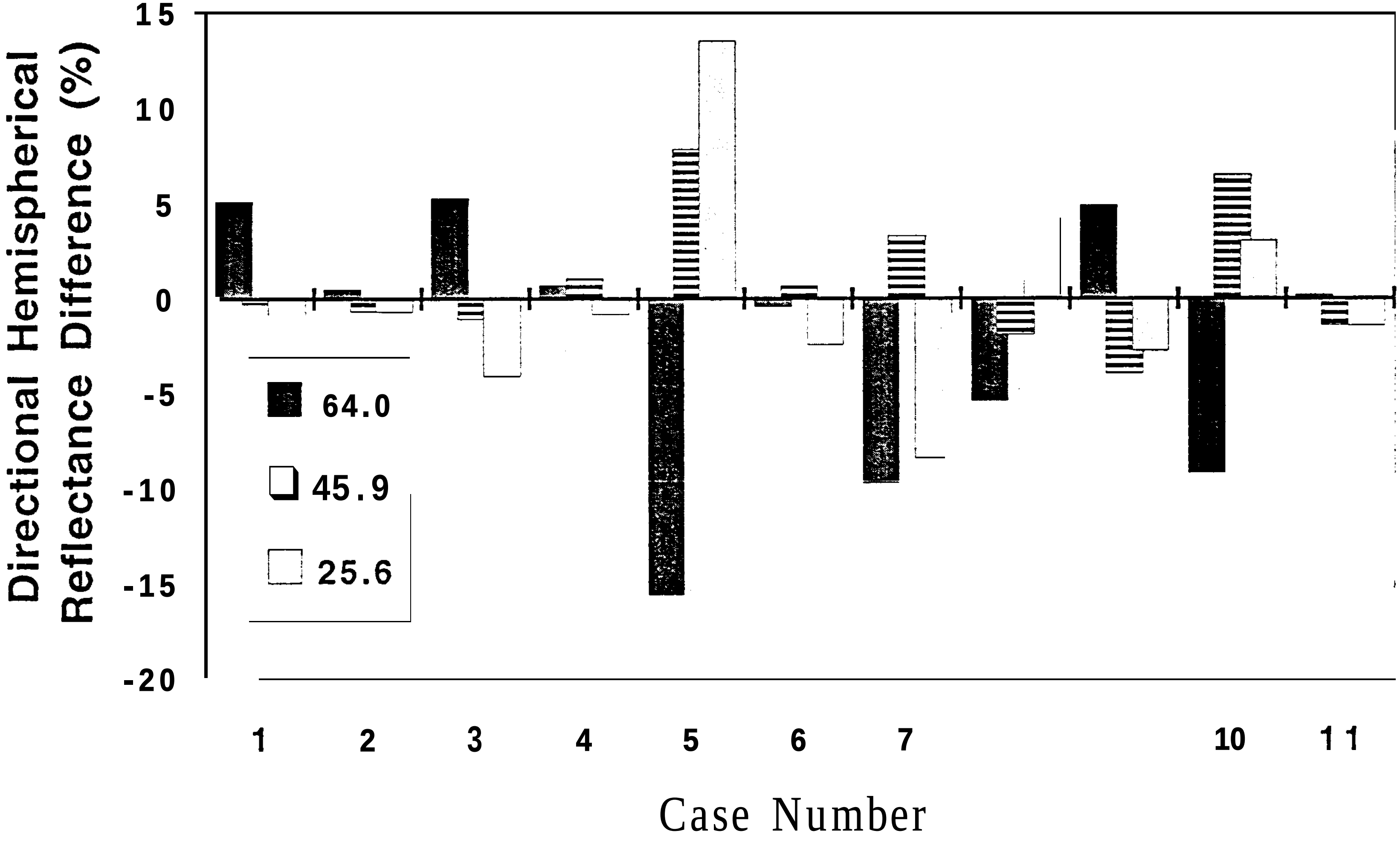

Directional Hemispherical Reflectance Difference (%)
15
10
5
0
-5
-10
-15
-20
64.0
45.9
25.6
1
2
3
4
5
6
7
10
11
Case Number

Figure 10

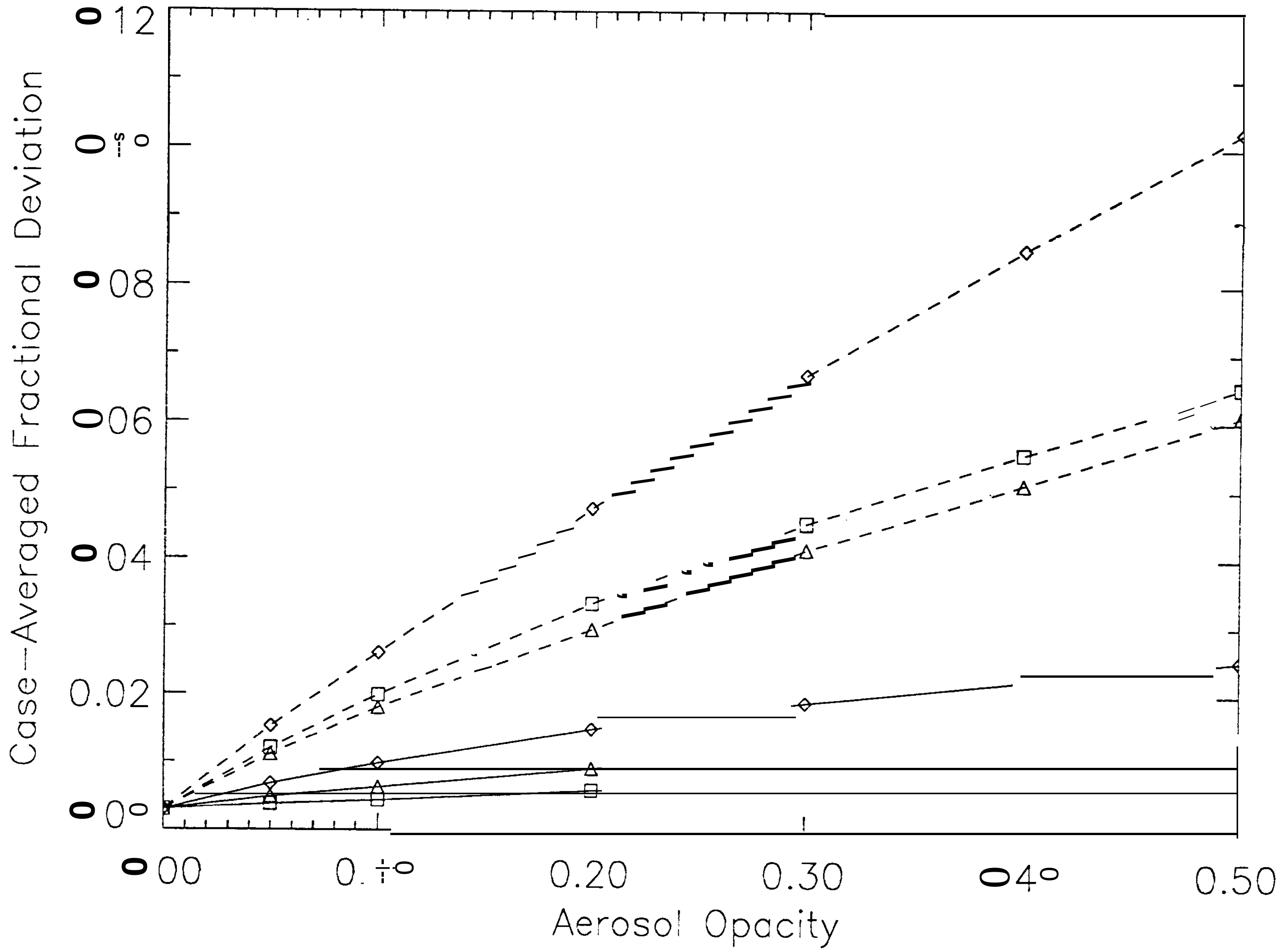
Case-Averaged Fractional Deviation
0.02
Aerosol Opacity
0.20
0.30
0.50

Figure 11

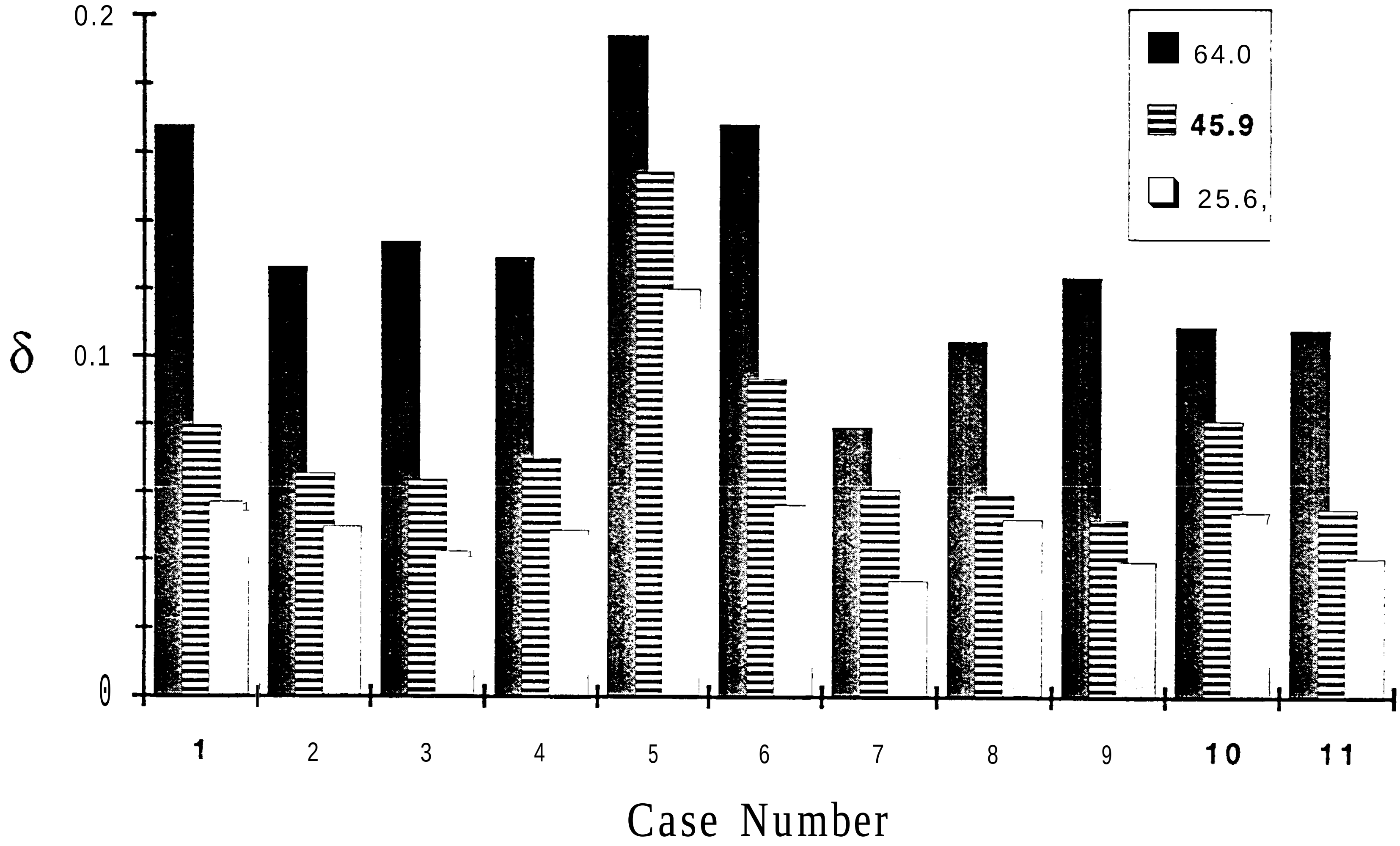

Figure 12

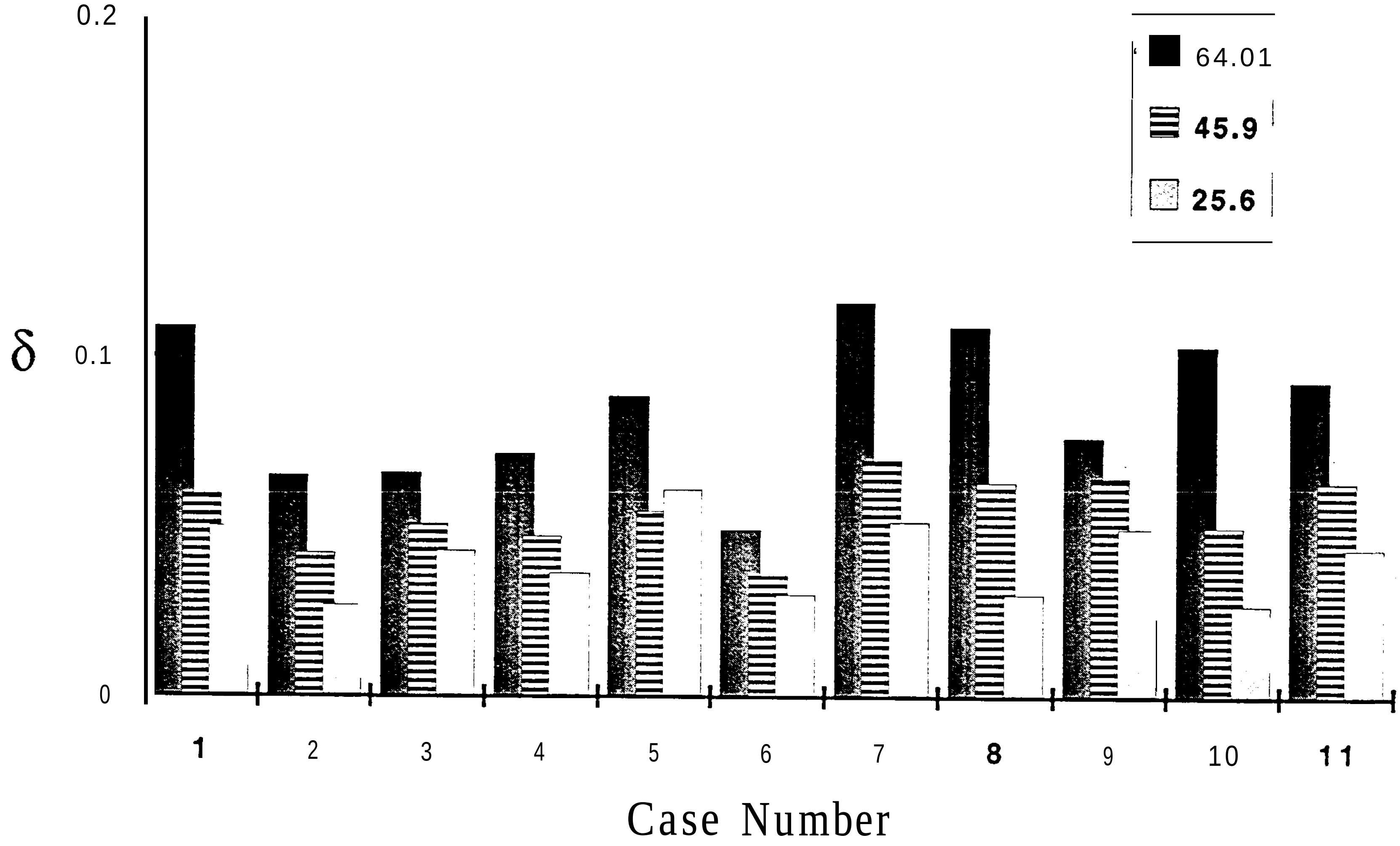

Figure 13

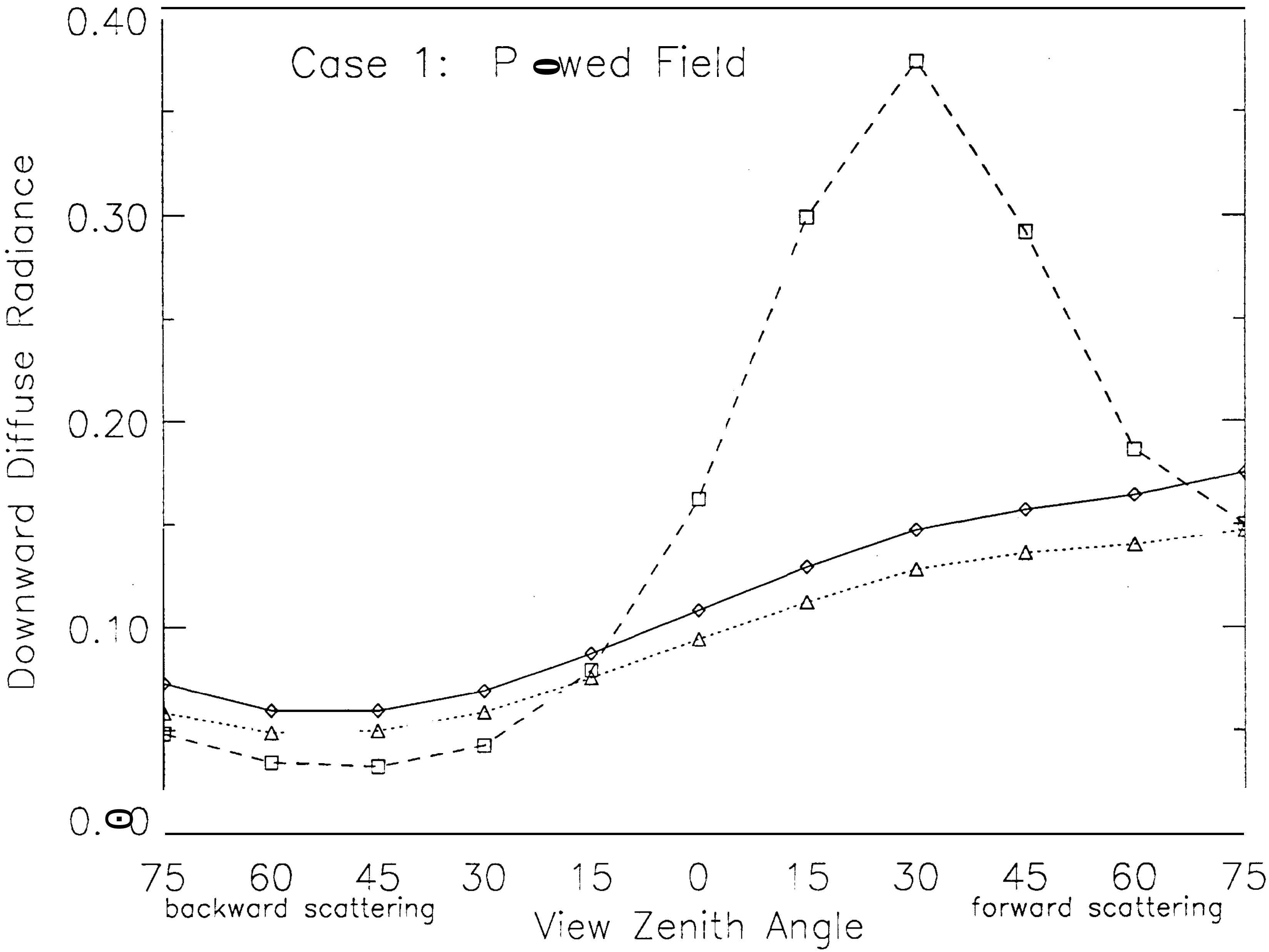
Case 1: P owed Field
Downward Diffuse Radiance
0.40
0.30
0.20
0.10
0.00
75 60 45 30 15 0 15 30 45 60 75
backward scattering
forward scattering
View Zenith Angle

Figure 14